A Hybrid SBR/MoM Technique for Analysis of Scattering from Small Protrusions on a Large Conducting Body

Jian-Ming Jin, *Senior Member, IEEE*, Feng Ling, *Student Member, IEEE*, Shawn T. Carolan, Jiming M. Song, *Member, IEEE*, Walton C. Gibson, Weng Cho Chew, *Fellow, IEEE*, Cai-Cheng Lu, *Member, IEEE*, and Robert Kipp, *Member, IEEE*

***Abstract*— A hybrid technique combining the shooting-and-bouncing-ray (SBR) method and the method-of-moments (MoM) is presented for analyzing scattering by large conducting bodies having small protrusions. In this technique, the MoM with an approximate Green's function is used to characterize the small protrusions, yielding an admittance matrix, which, when multiplied with the incident field on the protrusions, yields the currents induced on the protrusions. The incident field in the presence of the large bodies is calculated using the SBR method. The field radiated by the currents on the protrusions is also calculated using the SBR method with the aid of reciprocity. Furthermore, an iterative approach is developed, which can reduce the error introduced by the use of the approximate Green's function. Numerical results are given to demonstrate the accuracy and capability of the hybrid technique.**

***Index Terms*— Electromagnetic scattering, geometrical theory of diffraction, moment methods.**

I. Introduction

FOR analysis of large-scale electromagnetic scattering problems, high-frequency asymptotic methods are fast but approximate, whereas low-frequency numerical methods are accurate but slow. Neither can produce an efficient and accurate solution to scattering by large bodies containing small structures. A promising approach is to combine the best features of both types of methods to produce a hybrid technique that is sufficiently fast, reasonably accurate, and applicable to a class of unsolvable problems such as the scatterers mentioned above. There are two extremes for this type of hybridization. One is simply to superimpose solutions from asymptotic and numerical methods. While this approach is most widely used in practical applications, it neglects the interactions between the two solutions, which can be significant in many problems. The other extreme is to combine an asymptotic and a numerical method in an exact manner, such as the classical work of combining the method-of-moments (MoM) with the geometrical theory of diffraction (GTD) by Thiele *et al.* [1]–[3]. In this approach, the effect of a large body is included by incorporating its diffraction into the Green's function in the integral equation for the small structures, which accounts for all interactions. The approach is particularly attractive for analyzing the radiation of an antenna placed on a large body and it has recently been extended to scattering by finned convex objects [4]. While this approach is accurate, it is difficult to implement in a general-purpose computer code because of its complex nature. A more practical approach is to develop a technique that can include all significant interactions and neglect all trivial interactions. A successful example is given in [5] and [6] where the shooting-and-bouncing-ray (SBR) method is combined with the finite-element method (FEM) to solve for the scattering and radiation by a large body with cracks and cavities on its surface. The resulting hybrid technique can produce sufficient accuracy and can be implemented in a general-purpose computer code. In this paper, we employ the same philosophy to develop a technique that combines the SBR method and the MoM to solve for the scattering by large conducting bodies with small structures mounted on their surfaces. We note that since the nature of this problem is different from that in [5], the formulation is also different. To be more specific, in the proposed technique, an integral equation is first derived for the currents in the entire object, including the large body and the small structure. By choosing a proper Green's function that satisfies certain boundary conditions on the surface of the large body, the integral equation is reduced to an integral equation over the surface of the small structure. Application of the MoM to this equation with an approximate Green's function yields an admittance matrix, which characterizes the small structure. When multiplied by the incident field on the small structure, which is calculated using the SBR method, the admittance matrix yields the currents on the small structure, which radiate in the presence of the large body. The radiated field from these currents or the scattered field contributed by the small structure is then calculated using the SBR method with the aid of the reciprocity theorem.

For most problems, the formulation described above can yield a satisfactory solution. However, for some problems, an approximate Green's function can be difficult to obtain and

Manuscript received September 30, 1997; revised June 12, 1998. This work was supported by a grant from AFOSR MURI under Contract F49620-96-1-0025, the National Science Foundation under Grant NSF ECE 94-57735, and the Office of Naval Research under Grant N00014-95-1-0848.

J.-M. Jin, F. Ling, S. T. Carolan, J. M. Song, W. C. Gibson, and W. C. Chew are with the Center for Computational Electromagnetics, Department of Electrical and Computer Engineering, University of Illinois at Urbana-Champaign, Urbana, IL 61801 USA.

C. C. Lu and R. Kipp are with DEMACO, Inc., Champaign, IL 61820 USA.

Publisher Item Identifier S 0018-926X(98)06875-6.

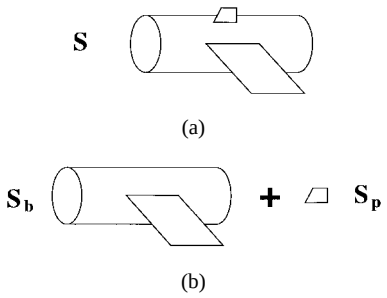

Fig. 1. (a) Original problem. (b) Decomposed problem.

the resultant solution can be rather inaccurate. In this case, the accuracy of the approximate solution can be improved using an iterative approach, similar to the methods employed in [7]–[9]. This iterative approach can also be applied to the case of multiple small structures having mutual interactions. As a result, although the hybrid technique presented is approximate, its accuracy can be improved systematically when necessary. This technique has been implemented successfully for two-dimensional scattering and yielded excellent results [10]. In this paper, we implement this technique for three-dimensional (3-D) scattering to evaluate its accuracy and capability.

II. The Hybrid SBR/MoM Technique

In this section, the basic principle of the hybrid SBR/MoM technique is described, followed by a discussion of the application of SBR and MoM in the hybrid technique.

A. The Basic Principle

Consider the problem of wave scattering by a large perfectly conducting body with a small protruding structure, illustrated in Fig. 1(a). The electric field satisfies the vector wave equation

$$\nabla \times \nabla \times \mathbf{E}(\mathbf{r}) - k_0^2 \mathbf{E}(\mathbf{r}) = -j\omega\mu_0 \mathbf{J}_i(\mathbf{r}) \tag{1}$$

where $\mathbf{J}_i$ denotes the source of the incident field. To find the electric field, we introduce the dyadic Green's function $\overline{\mathbf{G}}$, which satisfies the equation

$$\nabla \times \nabla \times \overline{\mathbf{G}}(\mathbf{r}, \mathbf{r}') - k_0^2 \overline{\mathbf{G}}(\mathbf{r}, \mathbf{r}') = \overline{\mathbf{I}}\delta(\mathbf{r} - \mathbf{r}') \tag{2}$$

and the Sommerfeld radiation condition. Multiplying (1) by $\overline{\mathbf{G}}$ and applying the vector-dyadic Green's theorem [11], we obtain the electric field integral equation (EFIE)

$$\mathbf{E}(\mathbf{r}) = \mathbf{E}^{inc}(\mathbf{r}) - j\omega\mu_0 \iint_S \overline{\mathbf{G}}(\mathbf{r}, \mathbf{r}') \cdot \mathbf{J}(\mathbf{r}')\, d\mathbf{r}' \tag{3}$$

where S denotes the surface of the entire scatterer, $\mathbf{J}$ is the surface current density induced on S, and $\mathbf{E}^{inc}$ represents the incident electric field given by

$$\mathbf{E}^{inc}(\mathbf{r}) = -j\omega\mu_0 \iiint_{V_s} \overline{\mathbf{G}}(\mathbf{r}, \mathbf{r}') \cdot \mathbf{J}_i(\mathbf{r}')\, d\mathbf{r}' \tag{4}$$

in which V_s denotes the volume occupied by $\mathbf{J}_i$. If $\overline{\mathbf{G}}$ is the free-space dyadic Green's function, $\mathbf{E}^{inc}$ is then the electric field produced by $\mathbf{J}_i$ in the free-space without the protrusion.

Equation (3) with the free-space dyadic Green's function provides the necessary integral equation for a MoM solution of $\mathbf{J}$ and then $\mathbf{E}$. However, since S includes the entire surface of the scatterer, a MoM solution of (3) requires the discretization of the entire surface, resulting in a very large number of unknowns for a large scatterer. As a result, the size of a scatterer to be handled by MoM is very limited because of the limitation of computer memory and time. To alleviate this limitation for the special scatterers considered here, we decompose the scatterer in Fig. 1(a) into two parts: one is the large body whose surface is denoted as S_b and the other is the small protrusion whose surface is represented by S_p, as illustrated in Fig. 1(b). Assuming that $\overline{\mathbf{G}}_b$ is a dyadic Green's function that satisfies the boundary condition

$$\hat{n} \times \overline{\mathbf{G}}_b(\mathbf{r}, \mathbf{r}') = 0 \quad \text{for } \mathbf{r} \text{ on } S_b \tag{5}$$

in addition to (2) and the Sommerfeld radiation condition, (3) then becomes

$$\mathbf{E}(\mathbf{r}) = \mathbf{E}_b^{inc}(\mathbf{r}) - j\omega\mu_0 \iint_{S_p} \overline{\mathbf{G}}_b(\mathbf{r}, \mathbf{r}') \cdot \mathbf{J}(\mathbf{r}')\, d\mathbf{r}' \tag{6}$$

and (4) becomes

$$\mathbf{E}_b^{inc}(\mathbf{r}) = -j\omega\mu_0 \iiint_{V_s} \overline{\mathbf{G}}_b(\mathbf{r}, \mathbf{r}') \cdot \mathbf{J}_i(\mathbf{r}')\, d\mathbf{r}'. \tag{7}$$

Clearly, $\mathbf{E}_b^{inc}$ is the electric field produced by $\mathbf{J}_i$ in the presence of the large body without the protrusion. Since S_p is small, (6) can be solved by MoM efficiently. The formulation described above can be readily applied to problems where the large body has one of the canonical shapes for which the dyadic Green's function is available. However, for a general shape of S_b, the explicit expression of $\overline{\mathbf{G}}_b$ is usually unknown. As a result, the MoM solution of (6) has three difficulties: 1) the required excitation $\mathbf{E}_b^{inc}$ cannot be calculated using (7); 2) the elements of the MoM impedance matrix cannot be computed; and 3) the field radiated by $\mathbf{J}$ cannot be evaluated even if $\mathbf{J}$ is obtained. In the following, we discuss the approaches to alleviate these difficulties.

B. The SBR Application

The first difficulty can be alleviated by using a different method to calculate $\mathbf{E}_b^{inc}$. Since $\mathbf{E}_b^{inc}$ is the incident electric field in the presence of the large body without the protrusion, it can be calculated efficiently and accurately using the SBR method with proper care.

The SBR method is a high-frequency technique for computing scattering of electromagnetic waves by electrically large bodies [12]–[14]. In the method, a dense grid of rays, typically 10–20 rays per wavelength representing the incident field, is launched toward the target. Each ray is traced as it bounces around within the target region and is governed by the geometrical optics (GO). At the last hit point or at each and every hit point, a physical optics (PO)-type integration is performed to determine the ray contribution to the scattered field. The total scattered field is the summation of

the contributions from all the rays. The SBR method has been implemented into a computer code, known as XPATCH [15], which can compute the radar cross section (RCS) of realistic 3-D targets. Although the SBR method can be employed directly to calculate $\mathbf{E}_b^{inc}$ on S_p, it can be time consuming since the total computing time is proportional to $O(nN_{ray1}N_{tri})$, where N_{ray1} denotes the number of rays that hit the large body (S_b) and N_{tri} denotes the number of triangular elements resulting from the MoM discretization of the protrusion (S_p), and n denotes the number of MoM integration points within each triangular element (typically from three to seven). A more efficient method is to trace each ray and when a ray passes through a triangular element on S_p (remember that the protrusion has been removed), its contribution to the field at the integration points on that element is calculated. Doing this, the computing time can be reduced to that proportional to $O(N_{ray1})+O(nN_{ray2}N_{tri})$, where N_{ray2} denotes the number of rays that hit the protrusion. The implementation of this approach, however, has a problem, as explained below. In practical applications, most targets have curved surfaces, instead of planar surfaces. When a curved surface is represented by a facet model, each facet actually represents a small portion of the curved surface, although each facet itself is flat or planar. Thus, when a ray hits one of these curved facets, its reflecting ray tube must either converge (when reflected from a concave surface), diverge (when reflected from a convex surface), or do a combination of the two (when reflected from a saddle point) in order to accurately model the physics. Neglecting the effect of the curved facets on ray tubes will lead to an erroneous calculation of the near field, though its effect on the far field calculation is insignificant since the latter is calculated by integrating the surface field as described above. This problem is illustrated in Fig. 2(a), where a plane wave is incident on a circular cylinder from the left side. Clearly, the reflecting ray tubes fail to cover the entire space and there are large gaps between the adjacent ray tubes. A simple method to solve this problem is to multiply each ray tube with a diverging factor determined at the hit point of the center of the tube, so that each ray will diverge as it leaves the curved surface. This method works satisfactorily for a surface having the same curvature such as a cylindrical and spherical surface. However, most curved surfaces have different curvatures at different points. For such surfaces, the simple method described above still leads to gaps or false overlapping between adjacent ray tubes, resulting in errors in the near field calculation. To solve this problem, instead of tracing the centerline of a ray tube and determining the reflecting direction and diverging factor based on the hit point of the center of the ray tube, we trace the four corner rays of a ray tube separately. Each corner ray is reflected into the direction based on its hit point and the reflecting ray tube is then formed by connecting the four corners. The diverging factor used to calculate the field is determined from the ratio of the cross section of the ray tube at the field point to its original size. The detailed implementation of this method is described by Carolan and Jin [16]. When this method is applied to the problem in Fig. 2(a), the reflecting ray tubes are shown in Fig. 2(b), yielding a very satisfactory result in the near field calculation.

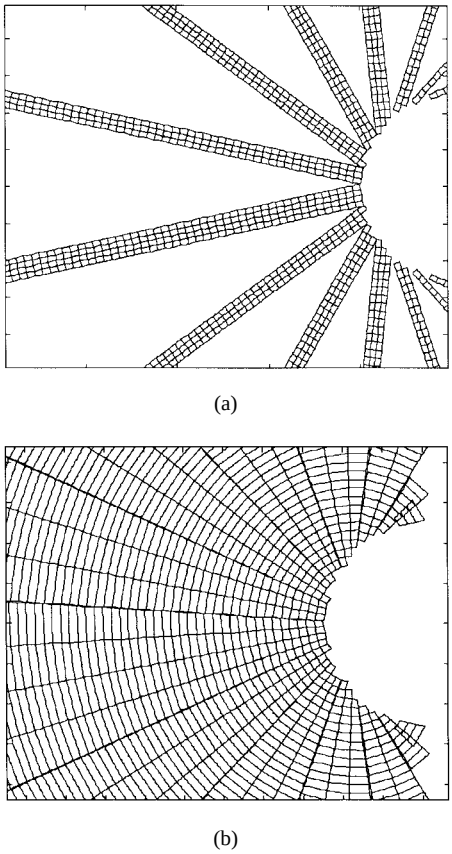

(a)

(b)

Fig. 2. Ray tube coverage reflecting from a cylinder. (a) Divergence off. (b) Divergence on.

As it turns out, the procedure described above works well in most cases, but some problems arise due to finite round-off errors in the computations. Ideally, the grid of ray tubes shot into the scene is intended to uniformly cover the space, but in cases where a point lies on or very near the border of two ray tubes, it can often be either double-counted (hit by two adjacent ray tubes) or missed completely. This can lead to inaccurate field calculations. The solution to this problem is to redefine the ray tube and introduce ray-tube basis functions. Instead of having a grid of barely touching ray tubes with a constant magnitude within each ray tube, the new ray tubes are defined with twice the width and the height so that the ray tubes are overlapping. To ensure a uniform field, a ray-tube basis function is then introduced such that at any point in space the contribution from all overlapping tubes add up to unity. This basis function can be written as $f(u,v) = (1-|u|)(1-|v|)$ for a ray tube extends over $-1 \leq u \leq 1$ and $-1 \leq v \leq 1$ in normalized ray-tube coordinates. Clearly, the magnitude is one at the center of the ray tube and varies to zero at the edges of the tube. With this modification, we can calculate accurately the field reflected to S_p by the large body.

In addition to the reflected field, another major contribution to $\mathbf{E}_b^{inc}$ is the direct illumination (zero bounce). This field can be calculated efficiently by launching a ray from the field point on S_p toward the source. If the ray is not intercepted by the large body, the field point is directly illuminated and a direct incident field is then added to that point.

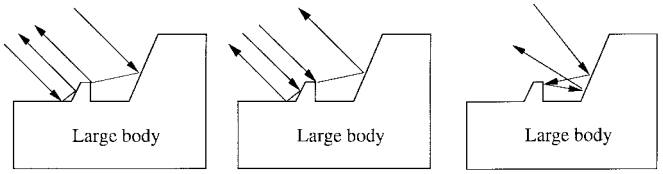

Fig. 3. Effects included in the hybrid technique: direct and indirect incident fields and direct and indirect scattered fields.

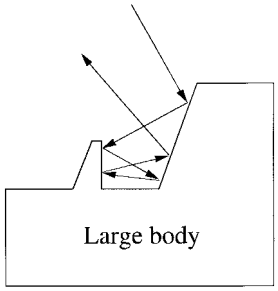

Fig. 4. Effects not included in the hybrid technique, but can be recovered by an iterative approach: field scattered by the protrusion, diffracted and/or reflected back to the protrusion by the large object, and scattered by the protrusion again.

C. The MoM Application

As mentioned above, the second difficulty caused by the lack of a closed-form expression for $\overline{\mathbf{G}}_b$ is in the evaluation of the elements of the MoM impedance matrix. To alleviate this difficulty, we first consider the role of $\overline{\mathbf{G}}_b$ in the MoM solution. To solve (6) by MoM, we apply it on S_p and take the cross product with the normal of S_p, yielding

$$j\omega\mu_0\hat{n}\times\iint_{S_p}\overline{\mathbf{G}}_b(\mathbf{r},\mathbf{r}')\cdot\mathbf{J}(\mathbf{r}')\,d\mathbf{r}' = \hat{n}\times\mathbf{E}_b^{inc}(\mathbf{r}) \text{ for } \mathbf{r} \quad \text{on } S_p. \tag{8}$$

Since both $\mathbf{r}$ and $\mathbf{r}'$ are on S_p, the $\overline{\mathbf{G}}_b(\mathbf{r},\mathbf{r}')$ in this equation represents the interaction between the two points on the protrusion. This interaction includes three contributions. The first is the direct interaction between the two points (the field produced by the point source at $\mathbf{r}'$ reaches directly at $\mathbf{r}$) and this interaction can be represented by the free-space dyadic Green's function. The second is the interaction through the base (assuming locally flat) on which the protrusion is placed (the field produced by the point source at $\mathbf{r}'$ is reflected by the base to the point $\mathbf{r}$) and this interaction can be represented by the free-space dyadic Green's function with the $\mathbf{r}'$ replaced by the image point $\mathbf{r}_i'$. The combination of these two interactions can be represented by the half-space dyadic Green's function denoted as $\overline{\mathbf{G}}_{\text{half}}$. The third contribution is the interaction through the other parts of the large body such as the edges (the field produced by the point source at $\mathbf{r}'$ is diffracted by the edges to the point $\mathbf{r}$). We denote this interaction as $\overline{\mathbf{G}}_{\text{diff}}$, which is the difference between $\overline{\mathbf{G}}_b$ and $\overline{\mathbf{G}}_{\text{half}}$. Therefore, we have

$$\overline{\mathbf{G}}_b(\mathbf{r},\mathbf{r}') = \overline{\mathbf{G}}_{\text{half}}(\mathbf{r},\mathbf{r}') + \overline{\mathbf{G}}_{\text{diff}}(\mathbf{r},\mathbf{r}'). \tag{9}$$

Using a local coordinate system for the MoM analysis which places the $z=0$ plane on the base of the protrusion, $\overline{\mathbf{G}}_{\text{half}}$ is then given by

$$\overline{\mathbf{G}}_{\text{half}}(\mathbf{r},\mathbf{r}') = \left(\overline{\mathbf{I}}+\frac{\nabla\nabla}{k_0^2}\right)[g(\mathbf{r},\mathbf{r}')-g(\mathbf{r},\mathbf{r}_i')] + 2\hat{z}\hat{z}g(\mathbf{r},\mathbf{r}_i') \tag{10}$$

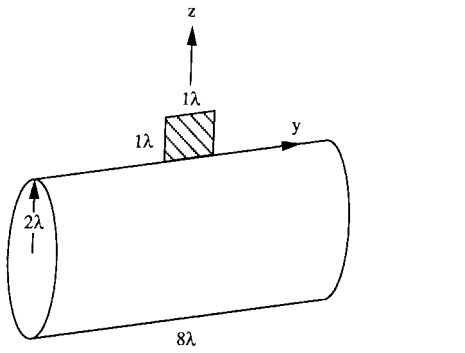

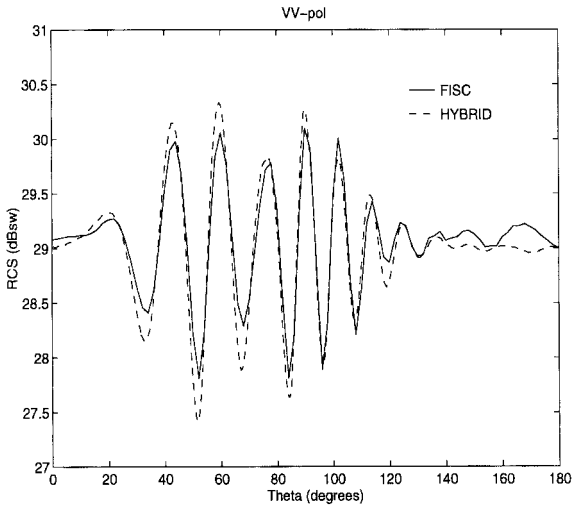

(a)

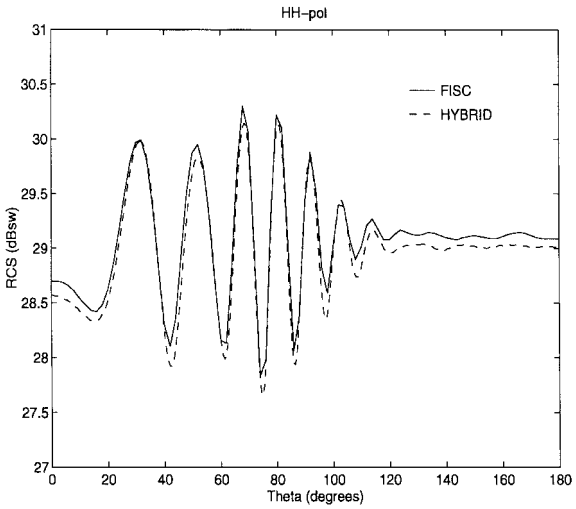

(b)

Fig. 5. Monostatic RCS of a plate attached to a finite circular cylinder in the xz plane. (a) Vertical (VV) polarization. (b) Horizontal (HH) polarization.

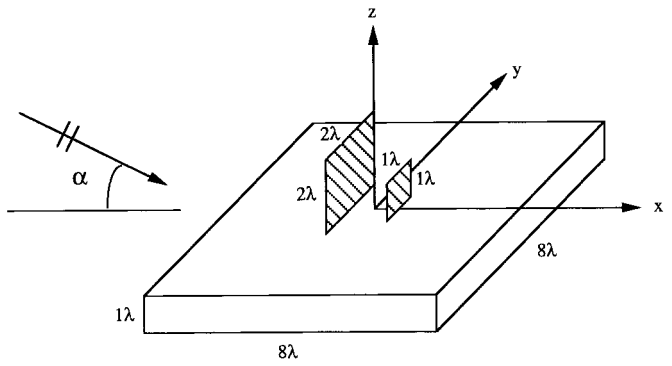

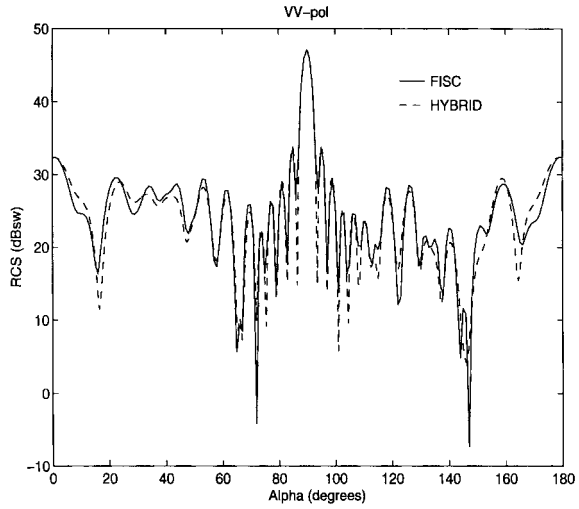

(a)

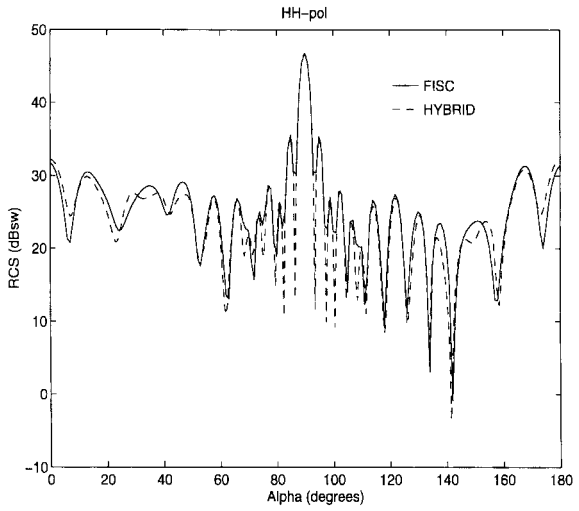

(b)

Fig. 6. Monostatic RCS of two small plates placed on a large thick plate in the xz plane (multiple interactions are included in the MoM solution). (a) VV polarization. (b) HH polarization.

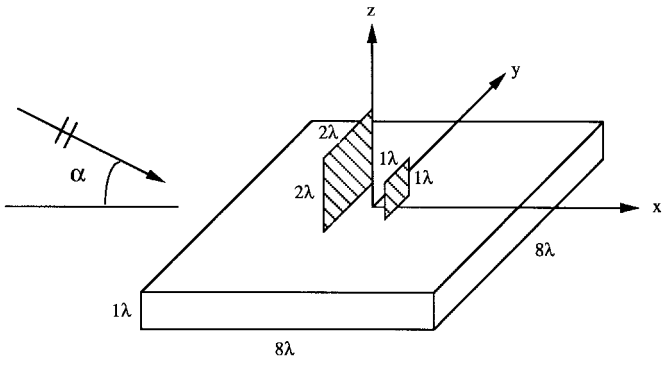

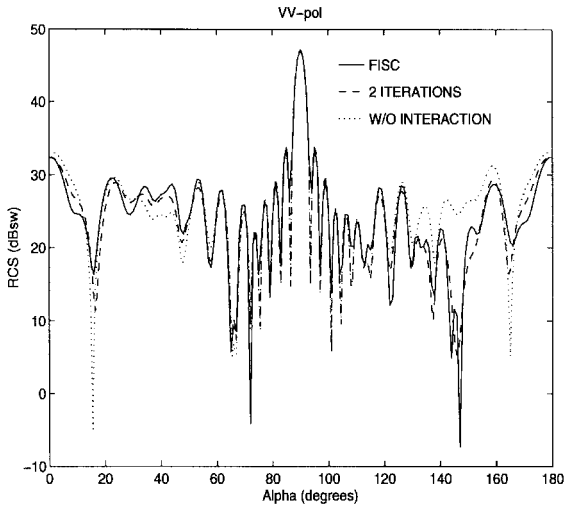

(a)

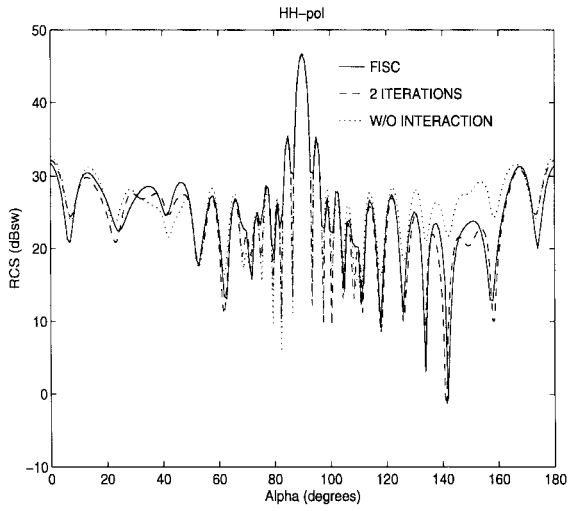

(b)

Fig. 7. Monostatic RCS of two small plates placed on a large thick plate in the xz plane (multiple interactions are not included in the MoM solution, but recovered by the iterative approach). (a) VV polarization. (b) HH polarization.

where $g(\mathbf{r}, \mathbf{r}') = e^{-jk_0|\mathbf{r}-\mathbf{r}'|}/4\pi|\mathbf{r}-\mathbf{r}'|$ and $\mathbf{r}_i' = x'\hat{x} + y'\hat{y} - z'\hat{z}$ denotes the image point of $\mathbf{r}' = x'\hat{x} + y'\hat{y} + z'\hat{z}$. Whereas the expression for $\overline{\mathbf{G}}_{\text{half}}$ is available, the expression for $\overline{\mathbf{G}}_{\text{diff}}$ is often difficult, if not impossible, to obtain. Although the effect of $\overline{\mathbf{G}}_{\text{diff}}$ can still be included in the MoM solution, as was done in [1]–[4], its numerical implementation is complicated and dependent on the geometry of the large object. To simplify the MoM solution and effectively decouple the MoM and SBR computations, we neglect $\overline{\mathbf{G}}_{\text{diff}}$ in the MoM solution of (8) and doing so we neglect the field scattered by the protrusion,

diffracted and/or reflected back to the protrusion by the large body and scattered by the protrusion again. In most cases, this field is unimportant. However, when necessary it can be recovered by using an iterative approach discussed in the next section. The MoM solution of (8) is straightforward. First, S_p is subdivided into small triangular elements and the current on S_p is expanded as

$$\mathbf{J} = \sum_{n=1}^{N} I_n \mathbf{f}_n(\mathbf{r}) \tag{11}$$

where N is the number of unknowns and $\mathbf{f}_n(\mathbf{r})$ denotes the vector basis functions. In this work, the Rao–Wilton–Glisson (RWG) basis functions [17] are used as $\mathbf{f}_n(\mathbf{r})$. In the usual MoM analysis, N includes only the interior edges; however, here N must include the boundary edges connecting the protrusion to the large body to allow the continuous flow of the current from the protrusion to the large body or vice versa. Applying Galerkin's method to (8) results in a matrix equation

$$[Z]\{I\} = \{V\} \tag{12}$$

whose elements are given by

$$\begin{aligned} Z_{mn} = {} & j\omega\mu_0 \iint_{T_m} \iint_{T_n} \\ & \cdot \left\{ \left[\mathbf{f}_m(\mathbf{r}) \cdot \mathbf{f}_n(\mathbf{r}') - \frac{1}{k_0^2} \nabla \cdot \mathbf{f}_m(\mathbf{r}) \nabla' \cdot \mathbf{f}_n(\mathbf{r}') \right] \right. \\ & \cdot [g(\mathbf{r}, \mathbf{r}') - g(\mathbf{r}, \mathbf{r}_i')] + 2\hat{z} \cdot \mathbf{f}_m(\mathbf{r}) \hat{z} \\ & \left. \cdot \mathbf{f}_n(\mathbf{r}') g(\mathbf{r}, \mathbf{r}_i') \right\} d\mathbf{r}' d\mathbf{r} \end{aligned} \tag{13}$$

$$V_m = \iint_{T_m} \mathbf{E}_b^{inc}(\mathbf{r}) \cdot \mathbf{f}_m(\mathbf{r})\, d\mathbf{r} \tag{14}$$

where T_m (or T_n) denotes the triangular elements covered by $\mathbf{f}_m$ (or $\mathbf{f}_n$).

D. Scattered-Field Computation

Once the surface current on the protrusion is obtained, the scattered field radiated by this current in the far zone can be evaluated using

$$\mathbf{E}^{sca}(\mathbf{r}) = -j\omega\mu_0 \iint_{S_p} \overline{\mathbf{G}}_b(\mathbf{r}, \mathbf{r}') \cdot \mathbf{J}(\mathbf{r}')\, d\mathbf{r}'. \tag{15}$$

Since $\mathbf{r}$ in this equation represents the observation point in the far zone, one cannot replace $\overline{\mathbf{G}}_b$ with $\overline{\mathbf{G}}_{\text{half}}$ because such a replacement would neglect the field scattered by the protrusion and diffracted and/or reflected to the observation point, resulting in an error whose magnitude is comparable to the field scattered directly to the observation point. There are two approaches to alleviate this problem. One approach is to first compute the field scattered by the protrusion over a small half-spherical surface enclosing the protrusion. This field is then converted into many rays which shoot along the radial directions. The contribution of each ray to the observation point is then calculated by the SBR method described earlier. This approach has the advantage of simultaneously computing the scattered field in all directions. However, to obtain accurate results the field on the half-spherical surface enclosing the protrusion must be divided into many rays and to trace each ray, its divergence factor must be calculated and tracked. Moreover, the process has to be repeated for each element in the protrusion. In this work, we use the second approach, which employs reciprocity theorem. In this approach, we place an infinitesimal electric current element at the observation point, either vertically polarized or horizontally polarized. We then compute the electric field $\mathbf{E}_{v,h}^{sbr}$ produced by this current element on S_p in the presence of the large body without the protrusion using the SBR method. In the backscatter case, $\mathbf{E}_{v,h}^{sbr}$ is the same as $\mathbf{E}_b^{inc}$. From the reciprocity theorem, the scattered field can be obtained as

$$E_{\theta,\phi}^{sca}(\mathbf{r}) = -\frac{j\omega\mu_0 e^{-jkr}}{4\pi r} \iint_{S_p} \mathbf{J} \cdot \mathbf{E}_{v,h}^{sbr}\, d\mathbf{r}'. \tag{16}$$

The total scattered field from the entire scatterer is the superposition of this field and the field scattered by the large body without the protrusion, which can be calculated efficiently and accurately using the SBR method.

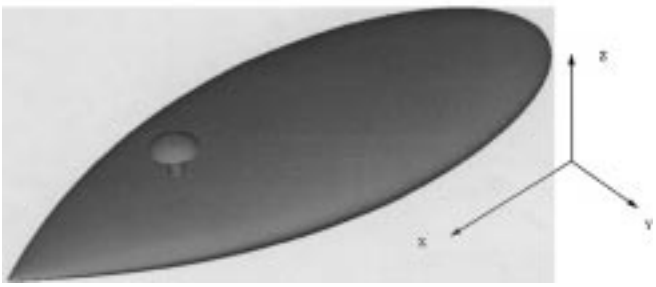

(a)

(b)

Fig. 8. (a) The almond (20 m long, 7.2 m wide, and 2.6 m thick) with a mushroom-shaped protrusion. (b) The VFY218 airplane (15.5 m long, 9 m wide, and 4.1 m thick) with a mushroom-shaped protrusion. The protrusion consists of a tapered circular disk, having a radius of 0.8 m and thickness of 0.6 m at the center, supported by a circular cylinder having a radius of 0.25 m and height of 0.7 m.

III. Iterative Improvement

Because of the use of the SBR method, $\mathbf{E}_b^{inc}$ in (6) includes not only the direct incident field, but also the fields multiply reflected by the large body. Generally speaking, the magnitude of the indirect incident field is comparable to that of the direct field, so neglecting either of them will result in a significant error in the calculation of $\mathbf{E}_b^{inc}$. Similarly, since

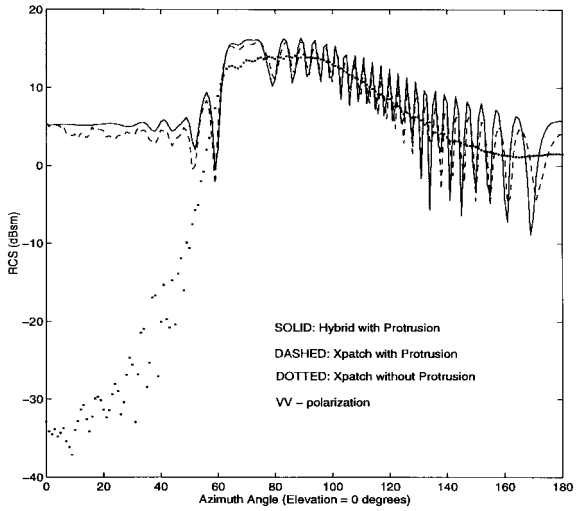

(a)

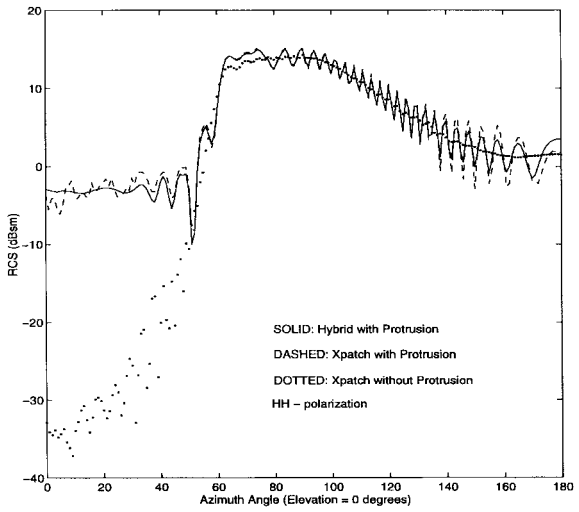

(b)

Fig. 9. Monostatic RCS of the almond with a mushroom-shaped protrusion at $f = 300$ MHz. (a) VV polarization. (b) HH polarization.

$\mathbf{E}_{v,h}^{sbr}$ in (16) is calculated using the SBR method, the reflection and multiple bounces are also included in the scattered-field calculation. Therefore, all major interactions, as illustrated in Fig. 3, between the SBR and MoM have been included in the hybrid technique.

The only approximation in the hybrid technique is introduced by the approximate Green's function, formed by neglecting the second term in (9). As pointed out earlier, this neglects the field scattered by the protrusion, reflected and/or diffracted back to the protrusion by the large object, and scattered by the protrusion again, as illustrated in Fig. 4. In most problems, this contribution is insignificant. However, when the protrusion is very close to edges and reflecting surfaces, this contribution can become significant and its omission can cause a substantial error in the solution. Here, we describe an iterative approach, similar to those in [7]–[9], to reduce the error systematically.

In this iterative approach, we use the current on the protrusion obtained from (12) as the initial value and then calculate the field produced by this current in the presence of the large body. This field can be considered as the secondary incident field, which, when superimposed to the $\mathbf{E}_b^{inc}$, yields a new incident field on the protrusion. Using this as the incident field in (14), we obtain a new improved current on the protrusion. This process is repeated several times until a stable value for the current is reached. The iterative process can be expressed as

$$\{I\}_i = [Z]^{-1}\{V[\mathbf{E}_b^{inc} + \mathbf{E}_b(\{I\}_{i-1})]\} \tag{17}$$

where i denotes the number of iteration, $\mathbf{E}_b(\{I\}_{i-1})$ denotes the field on the protrusion produced by the current $\{I\}_{i-1}$ on the protrusion, which can be calculated using either PO or the SBR method. A similar approach can be employed for large bodies with multiple protrusions. When each protrusion is characterized using the MoM, the interaction between them is neglected. To recover this interaction, we can first analyze protrusions separately and obtain the current on each protrusion. We then choose the current on one of the protrusions as the excitation to obtain the secondary incident fields on other protrusions, which then yield new currents. This process can be repeated until the convergence is reached. For the case with two protrusions, the process can be expressed as

$$\{I_1\}_i = [Z_1]^{-1}\{V_1[\mathbf{E}_1^{inc} + \mathbf{E}_1(\{I_2\}_{i-1})]\} \tag{18}$$

$$\{I_2\}_i = [Z_2]^{-1}\{V_2[\mathbf{E}_2^{inc} + \mathbf{E}_2(\{I_1\}_{i-1})]\} \tag{19}$$

where $\mathbf{E}_j(\{I_k\})$ denotes the field on the jth protrusion produced by the current on the kth protrusion, which can again be calculated using either PO or the SBR method.

IV. Numerical Results

To demonstrate the accuracy and capability of the proposed hybrid technique, we present some examples in which the incident wave is assumed to be a plane wave. In all the examples, the hybrid solution is compared to another independent solution.

The first example is a scatterer consisting of a $1\lambda \times 1\lambda$ plate placed on a finite circular cylinder having a diameter of 4λ and length of 8λ. The hybrid solution is compared to the MoM solution obtained by applying MoM to the entire scatterer. This MoM solution is calculated using the fast Illinois solver code (FISC) which implements the multilevel fast multipole algorithm (MLFMA) [18]. The results are given in Fig. 5, showing a good agreement between the two solutions.

The second example is a scatterer consisting of two plates of different size ($2\lambda \times 2\lambda$ and $1\lambda \times 1\lambda$, respectively) placed 1λ apart on an $8\lambda \times 8\lambda$ large plate having a thickness of 1λ. The hybrid solution is again compared to the result obtained using FISC and the comparison is shown in Fig. 6. Again, the agreement between the two solutions is good. In calculating the hybrid solution, we applied a single MoM to the two small plates or, in other words, the two small plates were treated as a single protrusion. As a result, the multiple interactions between the two small plates are included in the MoM solution.

To show the effectiveness of the iterative approach, we reconsider the second example. We first apply the MoM to each of the two plates independently and, hence, no interaction

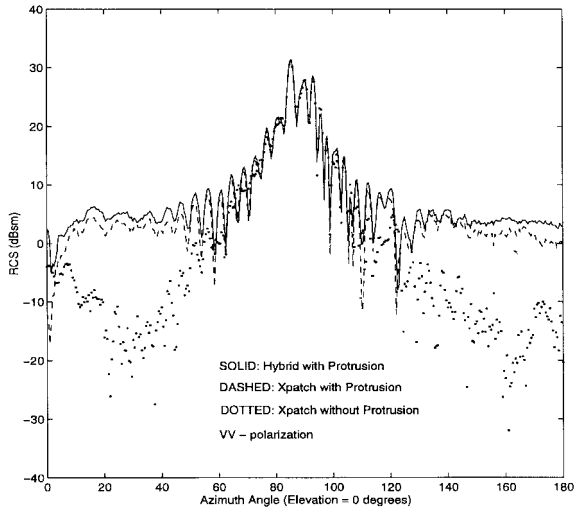

(a)

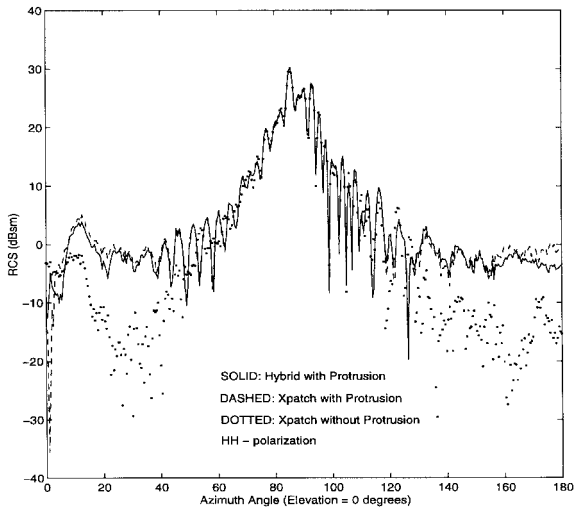

(b)

Fig. 10. Monostatic RCS of the VFY218 airplane with a mushroom-shaped protrusion at $f = 300$ MHz. (a) VV polarization and (b) HH polarization.

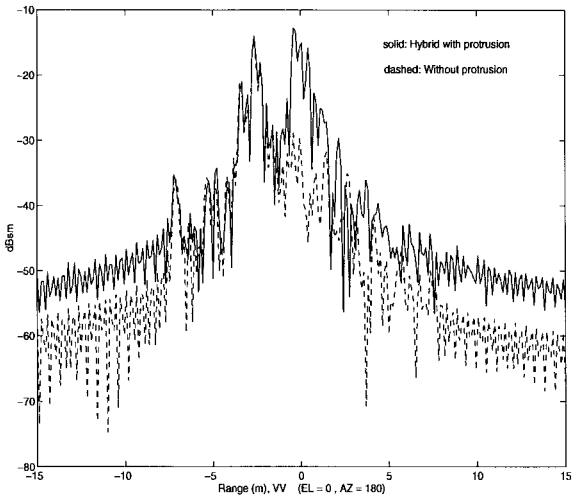

(a)

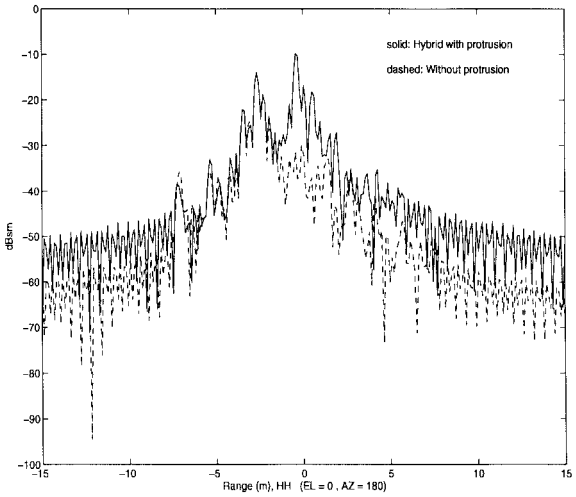

(b)

Fig. 11. Range profile of the VFY218 airplane with a mushroom-shaped protrusion for the head-on incidence. (a) VV polarization. (b) HH polarization.

between them is included. The hybrid solution so obtained is represented by the dotted line in Fig. 7, which shows a significant disagreement with the FISC result, especially in the region between 130° and 160°, because of the strong multiple interactions. This error is, however, reduced significantly when the iterative approach is applied with only two iterations. The result is shown by the dashed line which agrees with the FISC solution very well.

In the next two examples, the protrusion is a geometrically tapered circular disk supported by a small circular cylinder having a radius of 0.25 m and a length of 0.7 m. This object is placed on an almond and the VFY218 airplane, as shown in Fig. 8. The RCS of these two targets is given in Figs. 9 and 10, respectively. The hybrid solution is compared with the result obtained by XPATCH, which applies the SBR directly to the entire target. The two solutions agree remarkably well. It is evident in the almond case that the multiple interaction between the protrusion and the almond is predicted correctly. Also shown is the RCS of the two targets without the protrusion calculated using XPATCH. The results show that the protrusion has a significant contribution to the total RCS (30 dB in the almond case and 20 dB in the VFY218 case) in the low-observable directions. Finally, Fig. 11 gives the range profile of the VFY218 airplane with the protrusion for the head-on incidence.

V. Conclusion

A hybrid technique is presented for scattering by large bodies having small protruding structures. The technique invokes the equivalence principle to replace the protrusions with equivalent electric currents. The incident fields on the protrusions are calculated using the modified SBR method. The equivalent currents are then computed using the MoM method with an approximate dyadic Green's function. Finally, the scattered fields are evaluated using the SBR method with the aid of the reciprocity theorem. The hybrid technique combines the SBR method with the MoM in such a manner that the SBR and MoM computations are carried out separately and yet all significant interactions are included. For problems which require higher accuracy than the hybrid solution would give, an

iterative approach was designed to systematically improve the accuracy. The accuracy and capability of the hybrid technique were demonstrated using 3-D scattering examples.

REFERENCES

[1] G. A. Thiele and T. H. Newhouse, "A hybrid technique for combining moment methods with the geometrical theory of diffraction," *IEEE Trans. Antennas Propagat.*, vol. AP-23, pp. 62–69, Jan. 1975.

[2] E. P. Ekelman and G. A. Thiele, "A hybrid technique for combining moment method treatment of wire antennas with the GTD for the curved surfaces," *IEEE Trans. Antennas Propagat.*, vol. AP-28, pp. 813–839, Nov. 1980.

[3] L. W. Henderson and G. A. Thiele, "A hybrid MM-GTD technique for treatment of wire antennas near a curved surfaces," *Radio Sci.*, vol. 16, pp. 1125–1130, 1981.

[4] M. Hsu and P. H. Pathak, "Hybrid analysis (MM-UTD) of EM scattering from finned convex objects," in *IEEE Antennas Propagat. Soc. Int. Symp. Dig.*, Newport Beach, CA, June 1995, vol. 3, pp. 1456–1459.

[5] J.-M. Jin, S. S. Ni, and S. W. Lee, "Hybridization of SBR and FEM for scattering by large bodies with cracks and cavities," *IEEE Trans. Antennas Propagat.*, vol. 43, pp. 1130–1139, Oct. 1995.

[6] A. D. Greenwood, S. S. Ni, J. M. Jin, and S. W. Lee, "Hybrid FEM/SBR method to compute the radiation pattern from a microstrip patch antenna in a complex geometry," *Microwave Opt. Technol. Lett.*, vol. 13, pp. 84–87, Oct. 1996.

[7] D. S. Wang, "Current-based hybrid analysis for surface-wave effects on large scatterers," *IEEE Trans. Antennas Propagat.*, vol. 39, pp. 839–849, June 1991.

[8] U. Jakobus and F. M. Landstorfer, "Improved PO-MM hybrid formulation for scattering from three-dimensional perfectly conducting bodies of arbitrary shape," *IEEE Trans. Antennas Propagat.*, vol. 43, pp. 162–169, Feb. 1995.

[9] F. Obelleiro-Basteiro, J. L. Rodriguez, and R. J. Burkholder, "An iterative physical optics approach for analyzing the electromagnetic scattering by large open-ended cavities," *IEEE Trans. Antennas Propagat.*, vol. 43, pp. 356–362, Apr. 1995.

[10] F. Ling and J. M. Jin, "Hybridization of SBR and MoM for scattering by large bodies with inhomogeneous protrusions," *Progress Electromagn. Res. PIER 17*, 1997, pp. 25–43.

[11] C. T. Tai, *Dyadic Green Functions in Electromagnetic Theory*, 2nd ed. New York: IEEE Press, 1994.

[12] H. Ling, R. C. Chou, and S. W. Lee, "Rays versus modes: Pictorial display of energy flow in an open-ended waveguide," *IEEE Trans. Antennas Propagat.*, vol. AP-35, pp. 605–607, May 1987.

[13] H. Ling, R. C. Chou, and S. W. Lee, "Shooting and bouncing rays: Calculating the RCS of an arbitrary shaped cavity," *IEEE Trans. Antennas Propagat.*, vol. 37, pp. 194–205, Feb. 1989.

[14] J. Baldauf, S. W. Lee, L. Lin, S. K. Jeng, S. M. Scarborough, and C. L. Yu, "High frequency scattering from trihedral corner reflectors and other benchmark targets: SBR vs. experiments," *IEEE Trans. Antennas Propagat.*, vol. 39, pp. 1345–1351, Sept. 1991.

[15] D. J. Andersh, M. Hazlett, S. W. Lee, D. D. Reeves, D. P. Sullivan, and Y. Chu, "XPATCH: A high-frequency electromagnetic-scattering prediction code and environment for complex three-dimensional objects," *IEEE Antennas Propagat. Mag.*, vol. 36, pp. 65–69, Feb. 1994.

[16] S. T. Carolan and J. M. Jin, "Hybridization of the method of moments and the shooting-and-bouncing-ray method for scattering from large geometries with small protrusions," Univ. of Illinois, Urbana, IL, Res. Rep. CCEM-16-97, July 1997.

[17] S. M. Rao, D. R. Wilton, and A. W. Glisson, "Electromagnetic scattering by surface of arbitrary shape," *IEEE Trans. Antennas Propagat.*, vol. AP-30, pp. 409–418, May 1982.

[18] J. M. Song, C. C. Lu, and W. C. Chew, "MLFMA for electromagnetic scattering by large complex objects," *IEEE Trans. Antennas Propagat.*, to be published.

Feng Ling (S'97) was born in Jiangsu Province, China, in 1971. He received the B.S. and M.S. degrees in electrical engineering from Nanjing University of Science and Technology, Nanjing, China, in 1993 and 1996, respectively. He is currently working toward the Ph.D. degree in electrical engineering at the University of Illinois, Urbana-Champaign.

He has been a Research Assistant at the Center for Computational Electromagnetics at the University of Illinois, Urbana-Champaign, since 1996. His current research interests include numerical methods for electromagnetic scattering antenna and circuit problems.

Shawn T. Carolan received the B.S. and M.S. degrees from the University of Illinois at Urbana-Champaign, in 1996 and 1997, respectively.

He was a Research Assistant with the Center for Computational Electromagnetics, University of Illinois at Urbana-Champaign, in from 1996 to 1997, and worked for DEMACO, Champaign, IL, specializing in high-frequency electromagnetic modeling tools in 1997. He is currently a Software Engineer for Open Port Technology, Chicago, IL, specializing in internet telephony.

Jiming M. Song (S'92–M'95), for a photograph and biography, see p. 245 of the February 1997 issue of this TRANSACTIONS.

Walton C. Gibson recieved the B.S. degree in electrical engineering from Auburn University, Auburn, AL, in 1996. He is currently working toward the M.S. degree from the University of Illinois at Urbana-Champaign.

He is a Research Assistant at the Center for Computational Electromagnetics. His research interests include physical optics, shooting and bouncing rays, and ray tracing.

Weng Cho Chew (S'79–M'80–SM'86–F'93), for a photograph and biography, see p. 245 of the February 1997 issue of this TRANSACTIONS.

Cai-Cheng Lu (S'93–M'95), for a photograph and biography, see p. 543 of the March 1997 issue of this TRANSACTIONS.

Jian-Ming Jin (S'87–M'89–SM'94), for a photograph and biography, see p. 311 of the March 1998 issue of this TRANSACTIONS.

Robert Kipp (S'90–M'93), for a photograph and biography, see p. 132 of the January 1997 issue of this TRANSACTIONS.